Hindawi
Advances in Materials Science and Engineering
Volume 2023, Article ID 9891727, 1 page
https://doi.org/10.1155/2023/9891727

Retraction

Retracted: Analysis of Temperature Distribution and Mechanical Properties of Friction Stir Welding of Al-Cu Joints Using Hardened H13 Steel Tools

Advances in Materials Science and Engineering

Received 26 December 2023; Accepted 26 December 2023; Published 29 December 2023

This article has been retracted by Hindawi, as publisher, following an investigation undertaken by the publisher [1]. This investigation has uncovered evidence of systematic manipulation of the publication and peer-review process. We cannot, therefore, vouch for the reliability or integrity of this article.

Please note that this notice is intended solely to alert readers that the peer-review process of this article has been compromised.

Wiley and Hindawi regret that the usual quality checks did not identify these issues before publication and have since put additional measures in place to safeguard research integrity.

We wish to credit our Research Integrity and Research Publishing teams and anonymous and named external researchers and research integrity experts for contributing to this investigation.

The corresponding author, as the representative of all authors, has been given the opportunity to register their agreement or disagreement to this retraction. We have kept a record of any response received.

References

[1] J. Pratap Kumar, A. Raj, A. R. Venkatraman et al., "Analysis of Temperature Distribution and Mechanical Properties of Friction Stir Welding of Al-Cu Joints Using Hardened H13 Steel Tools," *Advances in Materials Science and Engineering*, vol. 2022, Article ID 4973839, 14 pages, 2022.

Hindawi
Advances in Materials Science and Engineering
Volume 2022, Article ID 4973839, 14 pages
https://doi.org/10.1155/2022/4973839

Research Article

Analysis of Temperature Distribution and Mechanical Properties of Friction Stir Welding of Al-Cu Joints Using Hardened H13 Steel Tools

J. Pratap Kumar,[1] **Anil Raj**,[1] **A. R. Venkatraman**,[2] **Arul Kulandaivel**,[3] **G. Ashwin Prabhu**,[4] **S. K. Narendranathan**,[3] **and Nagaraj Ashok**[5]

[1]*Department of Mechanical and Automobile Engineering, School of Engineering and Technology, CHRIST (Deemed to be University), Bengaluru-560074, Karnataka, India*
[2]*Department of Mechanical Engineering, Sona College of Technology, Salem, Tamilnadu, India*
[3]*Department of Mechanical Engineering, Agni College of Technology, Chennai-600130, Tamilnadu, India*
[4]*Department of Mechanical Engineering, St. Joseph's College of Engineering, Chennai-600119, Tamilnadu, India*
[5]*Department of Mechanical Engineering, Arba Minch University, Arba Minch, Ethiopia*

Correspondence should be addressed to J. Pratap Kumar; pratab@gmail.com and Nagaraj Ashok; nagaraj.ashok@amu.edu.et

Received 7 July 2022; Accepted 3 September 2022; Published 15 October 2022

Academic Editor: K. Raja

Friction Stir Welding (FSW) is a superior metal joining technique for joining similar and dissimilar metals. The various materials acceptable for the FSW techniques were magnesium alloys, mild steel, stainless steel, copper alloys, titanium alloys, aluminium alloys, etc. In this method, the frictional heat generated by the tool on metal workpieces was used for joining, and the workpieces were joined below the upper critical temperature. The substantial benefit of this technique is that it is capable of welding unweldable alloys by the conventional fusion welding method. The welding tool was rotated, traversed, and penetrated into the joint between two base plates. A suitable tool design with appropriate process parameters will result in high-quality welding on workpieces. In these experiments, the tools were designed with different pin profiles. The welding tools required for FSW are designed using SOLIDWORKS, and temperature distributions across the weld regions were analyzed using Ansys software. The fixture needed for FSW is fabricated according to machine requirements. The tool material used was hardened H13 steel, and the base plates were aluminium alloy 6101 and copper alloy C11000. The temperature distributions are noted in each trial during FSW of Al-Cu joints along the weld line region. Due to maximum temperature at weld joints, high ultimate tensile strength and impact strength were obtained at 1200 rpm tool rotational speed and 20 mm/min feed rate with the square pin profile of a hardened H13 steel tool. The obtained ultimate tensile stress (UTS) at joints was less than that of the base plates Al and Cu. The microhardness value was higher at the nugget zone than at the base plates, giving high strength at the joint area and unevenly distributed.

1. Introduction

Friction stir welding (FSW) is the method of joining two similar/dissimilar materials without using any consumable electrodes. Wayne Thomas invented this method in December 1991 at The Welding Institute (TWI) in Cambridge, UK. The FSW is a novel solid-state joining technique and has significant advantages compared to other standard welding techniques. The friction stir welding method uses a tool that rotates with shoulder and pin profiles embedded into the edges or surfaces of two workpieces in a butt joint configuration. The tool travels along the workpiece joint line [1–3]. In FSW, the welding tool rotation and tool progress directions determine the advancing and retreating side orientations. In recent years, this FSW process has been used in areas like marines, aerospace, aviation, automotive industries, fuel tanks, and other areas. Selection of the tool material, tool design, temperature distribution, mechanical

properties, and structural properties are the essential criteria in the FSW methods, which affect the weld characteristics, flow of plasticized material, uniformity, and strong consistency of the welded joint's robustness [4, 5]. It is possible to weld the alloy series using FSW methods. The selection of tool materials, tool pin configurations, and shoulder thickness were critical constraints in the FSW operation. The tool provides frictional heating of the workpieces and thermomechanical deformation below its recrystallization temperature. The FSW tool consists of a shoulder and a pin, which when they come into contact with the workpieces cause frictional and deformational heating. When the temperature at the joint line increases, that causes further extension of the softened material region. The various types of tool pin profiles are illustrated in Figure 1. The FSW tool pin profile impedes the plasticized material from escaping from the workpiece surface and appears to have a notable impact on the material flow at the weld joints [6].

In this paper, Chen and Kovacevic used 6061-T6 aluminium alloy by FSW in a butt joint configuration. The authors also examined the concept of stress and thermal evolution by employing a three-dimensional finite element method, which helps understand the FSW methods. The detailed model includes the tool shoulder's mechanical operation and the tool's thermomechanical effect (including shoulder and probe). This paper describes the weld's orthogonal stress evolution. The relationship between measured weld residual stresses and process parameters, including tool rotational speeds, welding speeds, and fixture discharge, was examined and conferred [7]. Ajit Kumar and Mallikarjuna conducted FEM model experiments on aluminium and copper plates using the friction stir welding method. In this experiment, welding process parameters such as tool rotational speed of 900 rpm and welding speed of 60 to 80 mm/min were adjusted. After that, thermal distributions were investigated for square and circular tool pin profiles. Creo software was used to build a finite-dimensional workpiece model with an FSW cutting tool joined by butt joint configurations and a thermal analysis concept [8]. Akbari et al. investigated the effects of friction stir welding tool configurations such as tool pin profile, shoulder diameter of the tool, length of the tool pin, axial force, feed rate, and temperature distribution analysis of friction stir welding of AA5083 aluminium alloy plates. The authors also determined the optimum tool pin diameter, height, and tool shoulder diameter. The FSW welding tool forces were evaluated using a specially set up dynamometer. Tensile strength was improved to examine the mechanical characteristics of the FSW welded joints [9]. Ghiasvand et al. discussed how the frictional heat distribution in the FSW process can be greatly affected by pin/tool offsets and the area of dissimilar alloy plates. The effects of the three parameters were studied, and the maximum temperatures of AA5086 and AA6061 aluminium alloy plates were examined. The authors found that pin offset is the most significant part of determining the maximum temperature reached when the AA6061 softer alloy was placed on the advancing side of both the pin and welding tool offset. The maximum temperature increment was greater than the retreating side of the harder alloy [10]. Aziz et al. used ANSYS

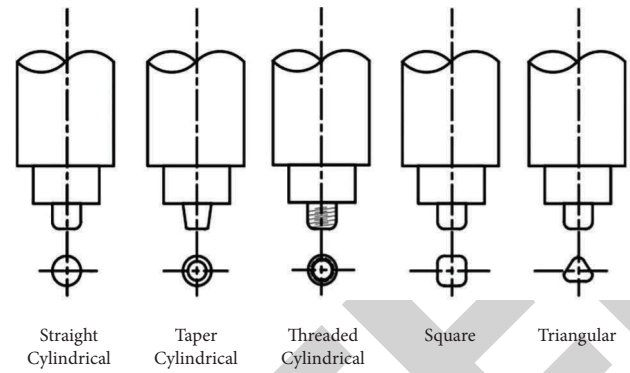

Figure 1: Illustrative diagram of different design of tool pin profiles [4].

APDL to generate a numerical thermomechanical model for the FSW. The impact of different weld process parameters on heat production during the welding process was studied. The model was confirmed by comparing experimental results with simulated temperature profiles from three different process welding conditions [11]. Jupri et al. discussed the effects of the tool tilt angle on the plates of aluminium AA5083 and copper C11000 FSW joints. The welding process parameters used in this experiment were tool rotation speed at 2500 rpm and feed rate at 30 mm/min. The mechanical and microstructure properties were performed to examine ultimate tensile strength values and metal movement properties toward the welded FSW of the Al-Cu welded joint. The authors found at 2 tilt angles, at 105 MPa, high tensile strength was obtained and the fracture surface was found nearly closer to Al and obtained brittle formation [12]. Anbukkarasi and Kailas used AA2024 and pure copper workpieces of 5 mm thick butt-welded configurations for various tool offset positions, with plain, threaded tool geometry, and plate positions. The authors found that welds with a smooth and continuous fresh interface had better properties than the welded joints with a nonuniform, intermittent interface. The tool geometry with a plain tool offset by copper placed at the advancing side welds has the best tensile strength due to constant metallurgical bonding at welds [13]. Yadav and Bhatwadekar used 5 mm thick plates of AA6101 aluminum and pure copper by butt joint weld configurations and used the H13 steel tool as an FSW tool with a cylindrical configuration design. The experiments were carried out at a tool rotational speed of 700 rpm and an 11 mm/min feed rate. In the stir region, the welded joint has an onion ring structure. They discovered that the AA6101 and copper joint were brittle by nature and that increasing the downward power, tool rotation speed, and welding speed resulted in a strong weld joint. The authors observed that the ultimate tensile strength of dissimilar joints was 93.2 MPa, which is less than the base metals. The AA6101-T6 was 284.4 MPa and the copper was 220 MPa [14]. Sharma et al. joined pure copper and AA5754 workpieces by FSW of butt weld configuration and an H13 steel tool was used. The structural, material flow, various pin profiles, and the hardness profile of the various welded joint areas were examined. The joints were prepared with different pin design configurations such as taper cam profile and square,

cylindrical, taper and cylindrical cam profile at a tool rotational speed of 900 rpm and a 40 mm/min feed rate. In all the FSW welded joints, the square tool pin profile allows regular joining at the nugget region, which increases the hardness, stronger joints, and microhardness. The material movement and microstructural investigations in the welding tool of square pin profile joints were examined in the longitudinal face to study the impact of stirring, including pulsating motion dissimilar to FSW [15]. Wei et al. used base plates AA1060 and pure copper T2 of 4 mm thickness. The authors revealed that tensile strengths were 102 MPa at a welding tool rotational speed of 950 rpm and an inclination of 0°. The microhardness values of the weld joint area were higher than those of the AA1060 and copper and irregularly dispersed [16]. Sadashiva and Shivanand used samples of size 55 mm × 10 mm × 5 mm. The Charpy test was used to study the impact strength of FSW joints. Due to moderate heat formation during the FSW at high speed and high feed rate, the authors found reverse characteristics of composite materials [17].

2. Experiment

2.1. Selection of Materials for FSW Process. In this experiment, the base materials used for FSW were AA6101 as the retreating side and C11000 as the advancing side for all the trials. The base plates AA6101 and C11000 have excellent electrical properties and play a vital role in major electrical applications such as electrical bus bars. The tool material was a hardened H13 steel tool with a square and round pin profile. The element distribution of base materials AA6101, C11000 plates, and FSW tool hardened H13 steel tool is displayed in Table 1 and 2.

2.2. CAD Modelling and Crafting of Tool and Baseplate. The dimensions of the two base plates were the same and set at 100 mm × 50 mm × 5 mm of length, width, and thickness, respectively. The 3-dimensional model of the base plate was illustrated in various views, as shown in Figure 2.

The tools were designed with one tool having a round pin profile and the other having a square pin profile. The rounded pin profiles were designed with a 20 mm diameter of the shoulder, a 70 mm length of shoulder, a 5 mm diameter of round pin, and a 5 mm pin depth. Square pin profiles were designed with a 5 mm × 5 mm size square pin and a 5 mm pin depth. The 3-dimensional model of the tool with a round pin profile and a 2-dimensional drawing of the same is shown in Figure 3.

The aluminium alloy 6101 and copper alloy C11000 plates were procured and the base plates were made as per the dimensions (100 mm × 50 mm × 5 mm of length, width and thickness), which are shown in Figure 4.

The H13 steel tool rods were procured and the tools with circular pin profiles and square pin profiles were made by machining as per the desired dimensions. After that, the tools were hardened by quenching, resulting in hardened H13 steel tools, as shown in Figures 5(a) and 5(b).

Table 3 shows the tool hardness of various pin profiles of the tool before and after hardness testing using the Rockwell Hardness test.

2.3. Experimental Setup for Carrying FSW Process in This Experiment. The experiments were performed using a vertical CNC milling machine by Skanda Mfg. System Pvt. Ltd. and temperature measurements were noted using an InfraRed thermometer (model: HTC IRX 68, temperature range:−50 to 1850°C, response time: 150 ms). The welding process was conducted in each trial with FSW process parameters such as feed rates and tool rotational speeds being computed in the CNC milling controller. In each trial, the weld joint temperatures were recorded from the initial to the end of the weld at every interval using an Infrared Thermometer [18, 19], as shown in Figures 5(c) and 5(d).

2.4. Selection of FSW Welding Process Parameters and Levels, FSW Tool Materials, FSW Tool Pin Profiles, and Base Plate Positions. The CNC milling machine used for the FSW process of joining AA6101 and C11000 plates uses a hardened H13 steel tool with a square and round pin profiles with a tool rotational speed range between 1000 and 1200 rpm with respective feed rates of 10, 15, and 20 mm/min. Each trial was conducted with a different tool rotational speed and feed rate. For instance, one trial with a 10 mm/min feed rate, a tool rotational speed of 1000 rpm, and a hardened H13 round tool pin profile. The setup fixed on the plates was C11000 was the advancing side and AA6101 was the retreating side. Table 4 shows the welding trial details.

2.4.1. Hardness Test. In this experiment, the Vickers microindentation hardness tester with a model VH1102 was used to test the microhardness of base plates Al and Cu. The hardness tester has a capacity of 10x and 50x and a magnification of 100x and 500x [20]. The tests were performed by fixing the load at 1 kg and a dwelling interval of 10 s for all the trials. The samples were prepared and tested according to the code ASTM E-384, as shown in Figure 6(a). To examine the tempering or solidification impacts of the FSW process on the aluminium and copper alloy plates. The microindentation analysis was conducted from the Al-Cu welded joint region to the base plates of Al and Cu. That was from the right side AS (Cu) base plate to the weld joint area of a distance of 5 mm each (+5 mm to 0 mm) and the left side base plate RS (Al) to the weld joint area of a distance of 5 mm each (−5 mm to 0 mm), as shown in Figure 6(b).

2.4.2. Tensile Strength Test. The specimens for the tensile test were processed using the wire EDM method essentially by the code ASTM E8-16a and specimen geometry was shown in Figure 7. In this tensile strength test, for each trial, an average of two specimens were applied. The tensile test was carried out using the TTM 5 tonnes capacity model.

Table 1: Element distribution of AA6101andC11000 in percentages from EDAX analysis.

Element	Al	Cu	Fe	Cr	Mg	Zn	Si	Ti	Mn	Ni	*P*	Pb	Bi	Ag	Sn
AA6101	93.95	0.21	0.29	0.08	1	0.18	4.02	0.14	0.12	—	—	—	—	—	—
C11000	—	94.36	0.35	—	—	0.49	1.07	—	0.22	0.28	0.21	0.96	1.02	0.57	0.47

Table 2: Element distribution of H13 steel tool in percentages from EDAX analysis.

Element	*C*	Cr	Fe	Mo	*S*	Sn	Ti	*V*	Si	Mn	*P*	Co	Ni	Cu	W
H13 steel tool	4.87	5.12	86.27	0.09	0.32	0.15	0.10	0.7	0.66	0.48	—	0.4	0.14	0.25	0.43

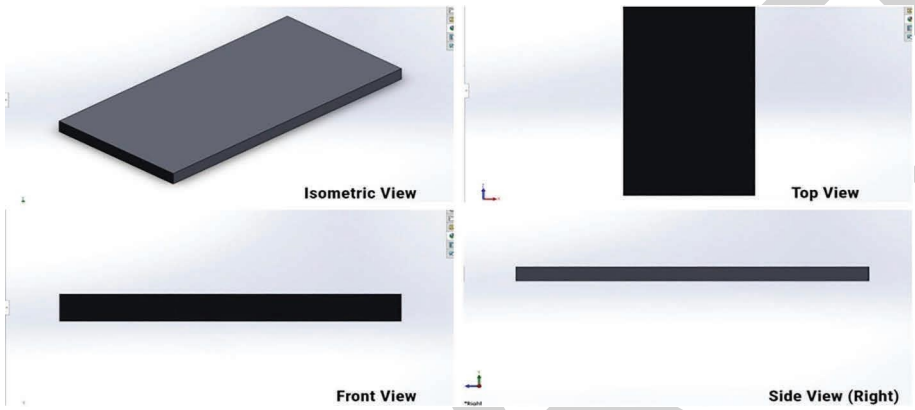

Figure 2: 3D model of base plate in different views.

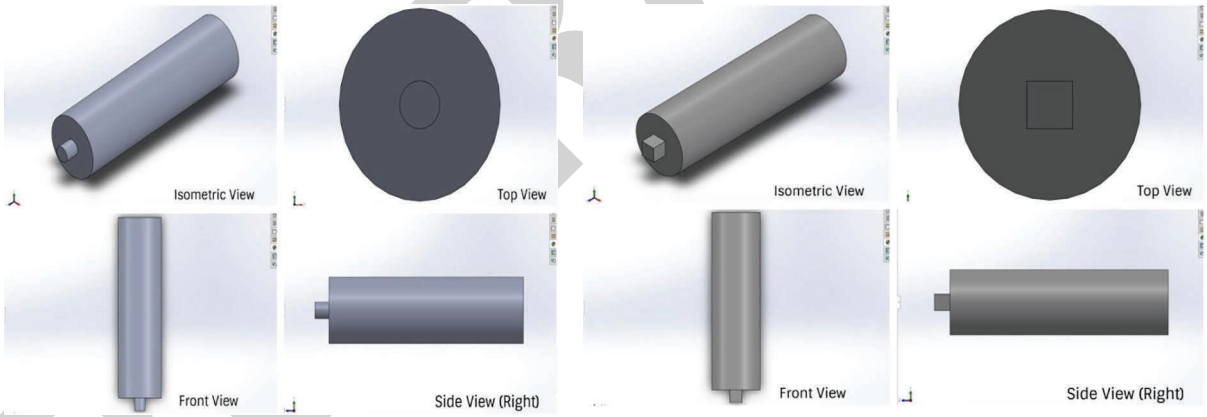

(a) (b)

Figure 3: 3D modelling of tool design (a) round tool and (b) square tool.

2.4.3. Charpy Impact Test. In this Charpy impact test, the rectangular shape of specimens with dimensions of 55 mm × 10 mm × 5 mm (length × width × thickness) was prepared using the wire EDM method as per ASTM E23. The V-Notch (model BMF-M) was made at the center of the weld joint exactly at 27.5 mm from the left/right (Rs-Al/As-Cu) side of the total length of 55 mm, as shown in Figure 8. In this test, an average of two specimens was taken to find out the impact strength of the specimen for each trial. The test was conducted on the model VI-30 Charpy impact test machine. The distance from the axis of rotation of the pendulum to the center of the specimen was 815 mm. The V-notched rectangular specimen is positioned at the center and then set within the two-terminal supports of anvils. The pendulum was free to fall from the height, hit the sample opposite the v-notch center, and measure the released height of the pendulum. The total energy absorbed by the specimen during fracture was tabulated.

3. Results and Discussions

3.1. Temperature Distribution Analysis of FSW Compared with Conventional Welding Techniques. The quality of the weld at each trial was observed and examined. The temperature at

Figure 4: Crafted plates of C11000 and AA6101.

(a)

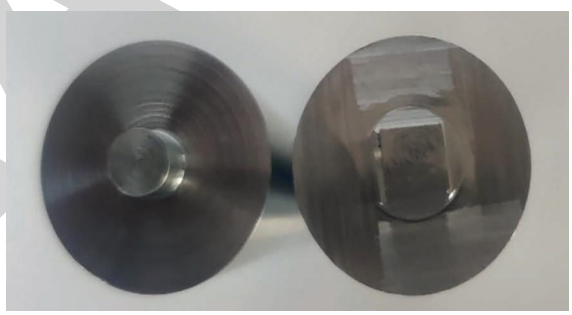

(b)

(c)

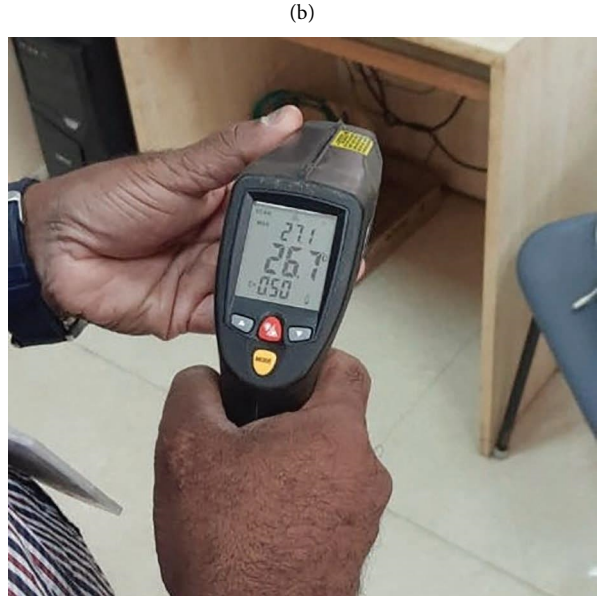

(d)

Figure 5: Hardened H13 steel tool with (a) round and square pin profiles. (b) Bottom section of the tools. (c) CNC milling machine. (d) Infrared thermometer.

Table 3: Hardness test of H13 steel tools.

Pin Profile	Before heat treatment	After heat treatment
Round	23HRC	55-61HRC
Square	23HRC	55-61HRC

Table 4: Various trials with respective welding tool rotation, feed rates, and tool pin profile.

Trial	Tool rotational speed (rpm)	Feed rate (mm/min)	Tool pin profile
1	1000	10	Round
2	1100	15	Round
3	1200	20	Square
4	1000	10	Square
5	1200	15	Square

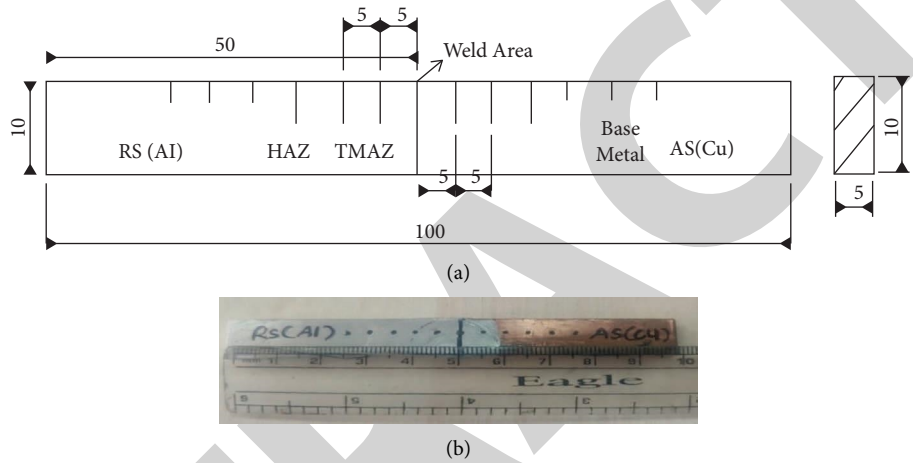

Figure 6: (a) Procedure for microindentation and (b) Sample preparation for microindentation.

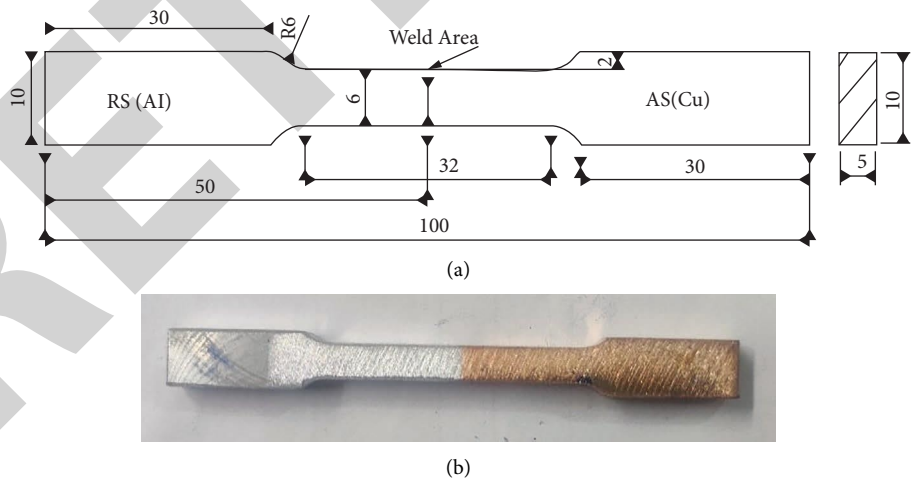

Figure 7: (a) Specimen geometry and (b) tensile test sample preparation.

the weld regions of 5 different trials, the maximum temperature, and the weld appearance after the FSW on base plates are shown in Tables 5 and 6, respectively.

Tables 5 and 6 illustrate that the welding region's temperature gradually increases in each trial. The maximum temperature out of the five trials was found to be 293°C in trial 3. This same trial yielded a better weld joint when the maximum tool rotational speed was set at 1200 rpm and the feed rate was 20 mm/min. The other four trials, 1, 2, 4, and 5, show the surface grooves due to low heat generation, minimum temperature distribution at the Al-Cu joints, and improper mixing at the joints. This movement was due to

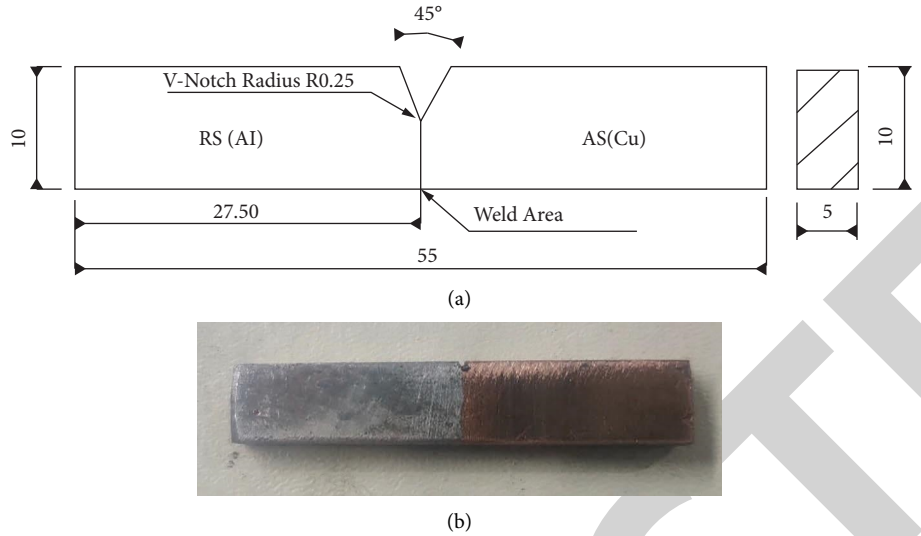

Figure 8: (a) Configuration of specimen preparation and (b) V-Notch sample preparation of Charpy impact test.

Table 5: Temperature at weld regions of each trial.

Trials	Temperature distributions at the weld region (°C)											
1	67.7	97.8	145.9	170.3	180.4	191.1	206.3	222	230.3	245.7	254.5	272.9
2	97.5	129.1	150.2	178	191.1	199.5	208.4	243	245.2	266.6	273	278.6
3	94	128.6	146	179.1	194.2	219.3	236	243.7	260	273.8	280	293
4	48.8	156.8	164	193	209.1	215	219	235.4	240	248	256	270
5	98.6	135.9	140.8	150.8	172.4	200.5	226.5	254.5	260.9	270.6	275	282

Table 6: Maximum temperature at weld regions of each trial and weld appearance after the FSW process.

Samples No	Tool rotational speed (rpm)	Feed rate (mm/min)	Max. temp at weld joints (°C)	Weld appearance
1	1000	10	272.9	
2	1100	15	278.6	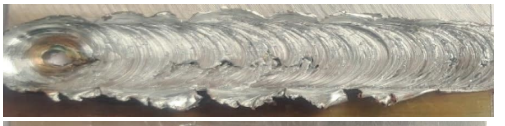
3	1200	20	293	
4	1000	10	270	
5	1200	15	282	

low tool rotational speed and feed rate. The readings show that the temperatures at the welding joints during the FSW process were lower than those of the traditional arc welding process.

3.2. Simulation of Welding Tool with Base Plates. The 3-dimensional models of the tool and base plates were exported from SOLIDWORKS in IGS file format. The material properties of the hardened H13 steel tools, AA6101, and C11000, were entered into the engineering database in the ANSYS workbench. The geometry is imported in IGS format and steady-state thermal is conducted. The materials were assigned to the tool and plates with a hardened H13 steel tool, C11000 and AA6101, respectively. The geometry models were meshed with an element size of 0.006 m, and the meshed models are shown in Figure 9. The initial temperature was set at 24°C and the tool temperature was set particularly for different trials as a boundary condition. The temperature distribution study of each trial was compared and analyzed as shown in Figure 10.

The simulations were conducted, and temperature distributions of geometry were observed in the ANSYS workbench. Figure 11 shows the temperature distribution of a hardened H13 steel tool with a round pin profile. The tool temperature was 272.9°C, which was set as a boundary condition and where the tool rotational speed was 1000 rpm and the feed rate was 10 mm/min. The initial temperature was set at 24°C, and the distribution between the plates and tools can be observed in the temperature contour plot.

Figure 12 shows the temperature distribution of the hardened H13 steel tool with a round pin profile and the tool temperature of 278.6°C, which was set as a boundary condition. The initial temperature was 24°C and the temperature contour plot illustrated was from the trial, where the tool rotational speed was 1100 rpm and the feed rate was 15 mm/min, which shows the distribution of the tools and workpieces.

Figure 13 shows the temperature distribution of the hardened H13 steel tool square with a pin profile and the tool temperature of 293°C, which was set as the boundary condition, and the initial temperature set at 24°C. This was the trial simulation with a tool rotational speed of 1200 rpm and a feed rate of 20 mm/min. The temperature contour plot can be observed with the temperature distributed between the tool and plates. The contour plots were analyzed and comparative studies were done along with conventional flame welding temperature distribution.

In this FSW process, the temperatures generated on the tools and workpieces were comparatively low. For comparison, various temperature distributions were simulated in the ANSYS workbench with different tool profiles and tool temperatures of the FSW process, along with the temperature distribution of the conventional flame welding process. The temperature distributions of the flame welding with a temperature of 1100°C were also simulated, which is shown in Figure 14 for comparison with Friction Stir Welding.

While comparing Figures 11 and 14, Figure 14 shows a temperature value of 845.16°C, which indicates that higher temperatures affect the structural integrity of the workpieces. In this case, the melting point of AA6101 is 654°C, and it is hard to weld the aluminium alloy by the fusion welding method. Figure 11 shows the minimum temperature value of 272.9°C. It illustrates that the heat-affected zone (HAZ) is the region where the metals do not get melted but their material properties get altered by heat generated during the FSW process. In this case, the temperature in the HAZ is lower compared with conventional flame welding. The FSW method was adopted to remove the flexible structural integrity of the workpieces. In FSW, as previously described, the welding occurs at a lower critical temperature for Al and Cu plates. Figures 12 and 13 also illustrate the respective HAZ of trials with 278.6°C and 293°C using hardened H13 steel tools with round and square pin profiles, respectively. It was also stated that heat input was high because of the maximum tool rotational speed and feed rate.

3.3. Mechanical Properties of the Al-Cu FSW Joints

3.3.1. Microhardness Measurements. Figures 15 and 16 show the microhardness curve and microindentation of the FSW joint plots of the first three trials. The tests were performed from the joints to the base metal at a 5 mm distance for each AS-Cu and RS-Al. The average microhardness value of the base plates Al and Cu obtained was 51.6 HV1 and 88.36 HV1 and at the Al-Cu joint was 104.63 HV1, which was higher than the value of base plates Al and Cu. On the Cu side, the average microhardness at the thermomechanically affected zone (TMAZ) was 74.83 HV1, and the HAZ was 84.86 HV1. This movement shows a decrease in HV1 value from the joint to the Cu base metal. On the Al side, the average microhardness at TMAZ was 77.1 HV1, and the HAZ was 72 HV1, which shows a decrease in HV1 value from the joint to the Al base metal. Hence, the microhardness appearance was random. Also, the microhardness value of TMAZ and HAZ of both the Al and Cu sides is lower than the Al-Cu joint area. This movement is because of increased tool rotational speed and feed rate, the effect of the thermal welding cycle, and microstructural variations made during the welding on aluminium and copper alloy plates. The microhardness of the nugget zone slightly increased.

3.3.2. Ultimate Tensile Strength Test (UTS). Figure 17 shows samples vs. UTS (MPa) and% of elongation, and Figure 18 shows samples vs. yield strength (YS) (MPa) and % of reduction area of the tensile test for FSW specimens of the first three trials. At a low speed of 1000 rpm and a feed rate of 10 mm/min with hardened H13 steel tool round configurations, the UTS was 85.77 MPa and the % of elongation was 7.06. The strain was 0.07 obtained. Young's modulus (E) was 1.22 GPa with a yield strength of 64.33 MPa and the % of reduction in the area of 0.65. This movement is due to inadequate heat input on the welded joint area, which causes surface groove defects, leading to low joint strength. At a medium speed of 1100 rpm, feed rate of 15 mm/min with hardened H13 steel tool round configurations, the UTS was 89.63 MPa and the % of elongation was 7.23. The strain was

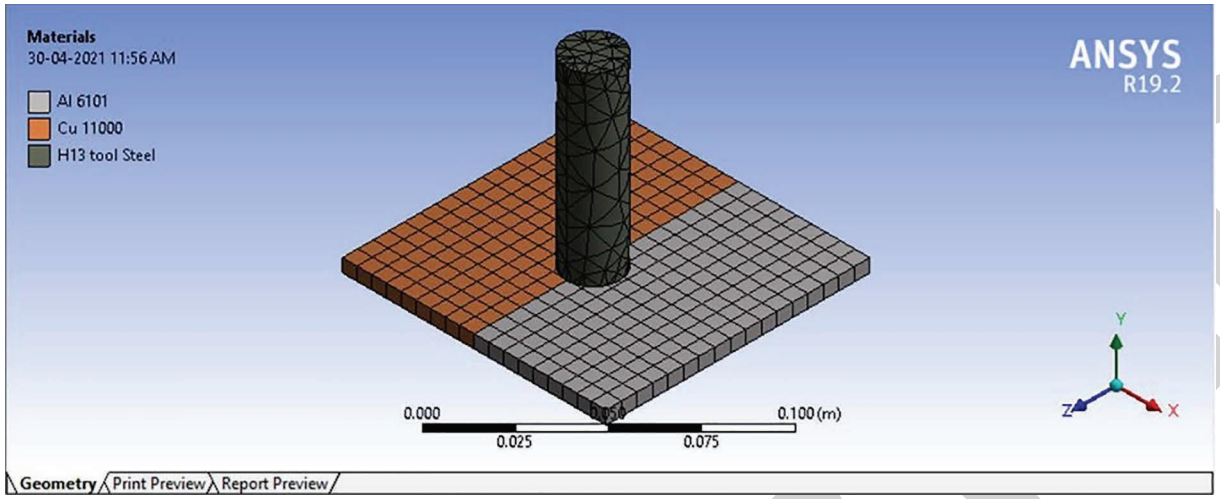

Figure 9: Meshing of geometry tool with base plates.

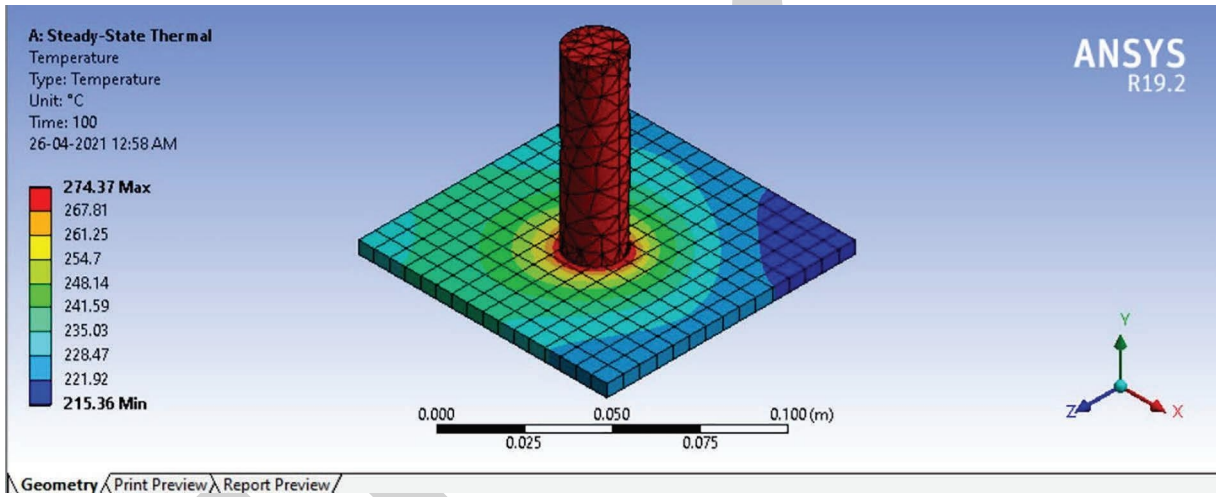

Figure 10: Temperature distribution.

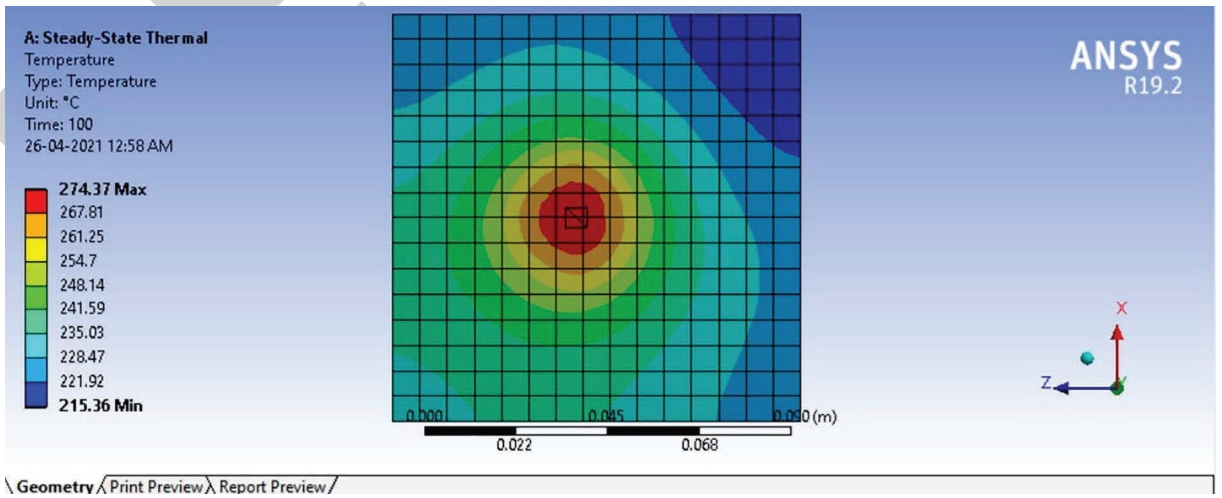

Figure 11: Temperature distribution with a hardened H13 steel tool round pin profile when tool temperature was 272.9°C.

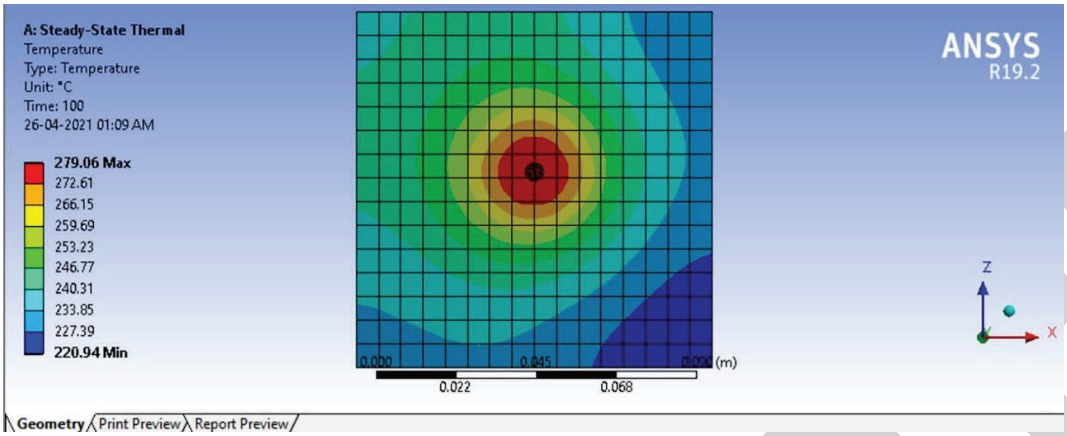

Figure 12: Temperature distribution with a hardened H13 steel tool round pin profile when tool temperature was 278.6°C.

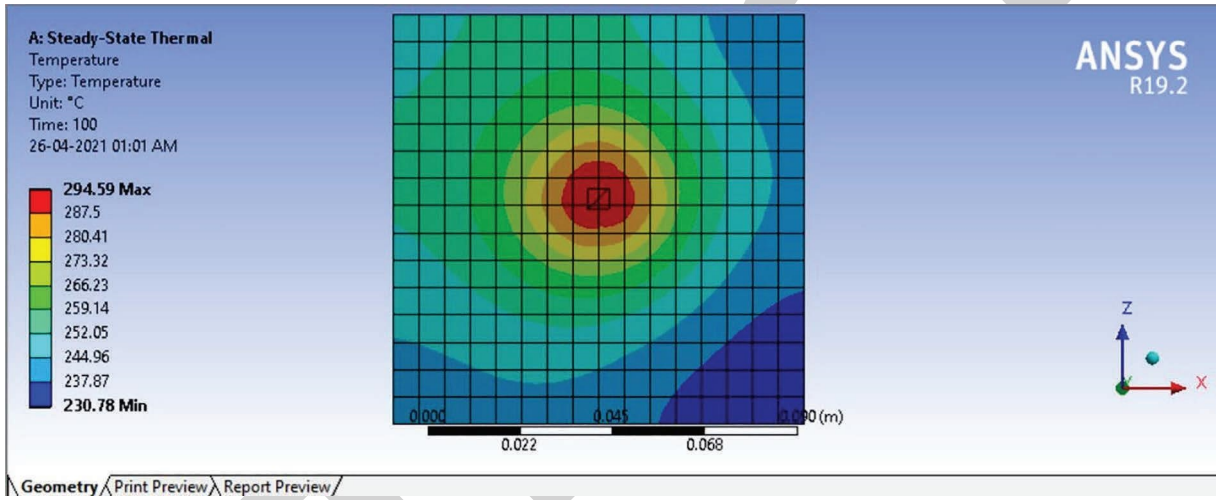

Figure 13: Temperature distribution with a hardened H13 steel tool square pin profile when tool temperature was 293°C.

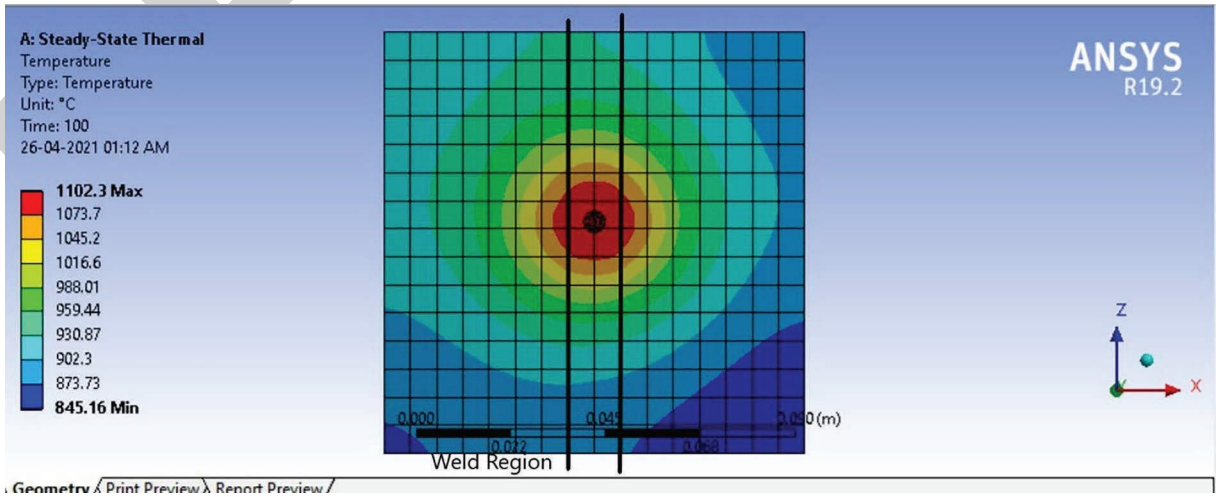

Figure 14: Temperature distribution of conventional flame welding when pin temperature is set at 1100°C.

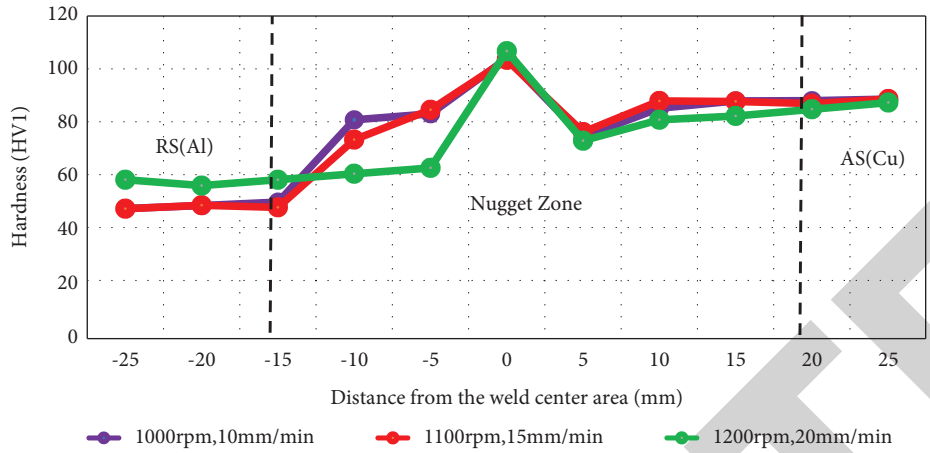

Figure 15: The microhardness distribution of welded joints at different tool rotation speeds and feed rates.

Figure 16: Vickers microhardness indentations: (Cu-AS) side: points 1–3 base metal area, points 3–6 HAZ and TMAZ, point 6 Al-Cu interface area (weld joint area), (Al-RS) side: points 6–9 TMAZ and HAZ, and points 9–11 base metal area (Al).

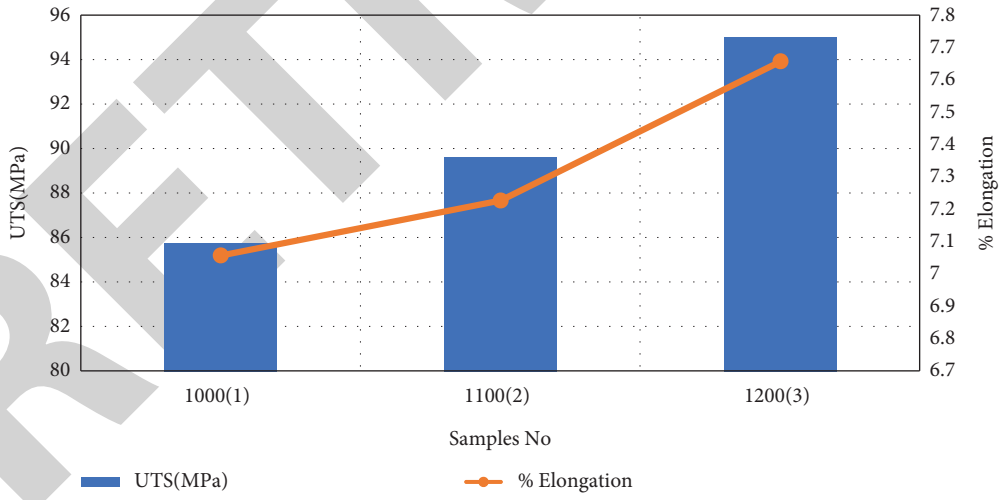

Figure 17: Samples vs. UTS (MPa) and % elongation.

0.0723. Young's modulus (E) was 1.24 GPa with a yield strength of 69.34 MPa and % of reduction in the area of about 0.5. At high-speed of 1200 rpm, feed rate of 20 mm/min with hardened H13 steel tool square configurations, the UTS was 95.04 MPa and the % of elongation was 7.66. The strain was 0.0766. Young's modulus (E) was 1.25 GPa with a yield strength of 74.38 MPa and % of reduction in the area of about 0.33. This movement was due to high tool rotational speed; maximum temperature causes removal of groove defects because of proper heat input caused by mechanical and metallurgical bonding effects; and more interfacial compounds were formed at the weld joint. The UTS value at the joint was less than the ultimate tensile strength of base plates Al and Cu. The joint efficiency increases when increasing the FSW process parameters such as feed rate and tool rotational speed.

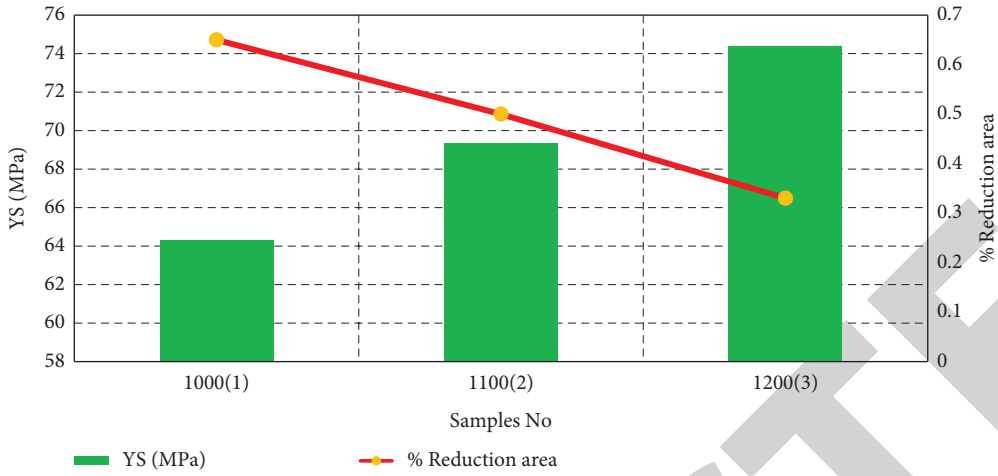

Figure 18: Samples vs. yield strength (MPa) and % reduction area.

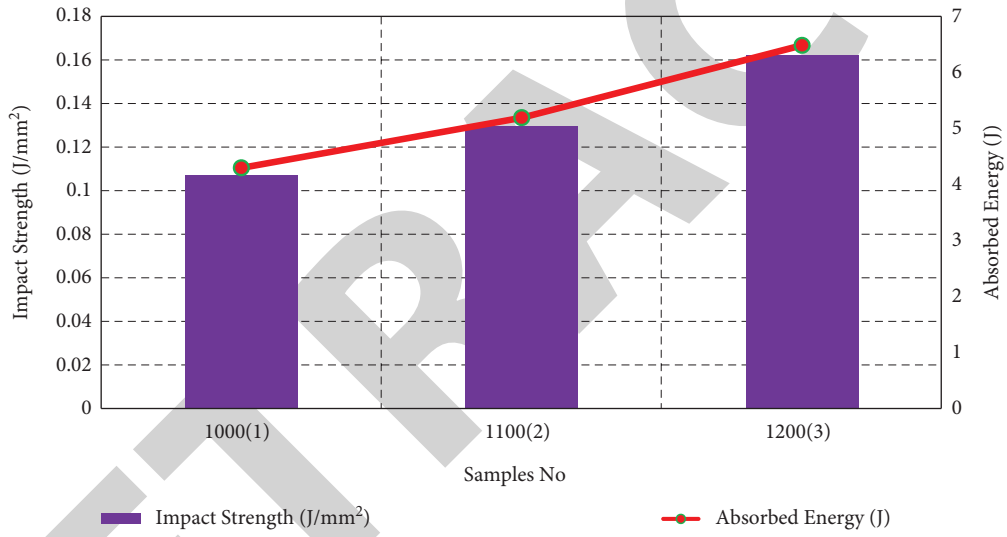

Figure 19: Samples vs. impact strength (J/mm^2) and absorbed energy (*J*).

3.3.3. Charpy Impact Strength Test. Figure 19 shows samples vs. absorbed energy (*J*) and impact strength of the specimen for the first three trials. The impact strength was low at 0.1075 J/mm^2 and 0.13 J/mm^2 at absorbed energy of 4.3 J and 5.2 J, when tool rotational speed was between 1000 and 1100 rpm and the feed rate was between 10 and 15 mm/min with hardened H13 steel tool round configurations. This movement is because of low heat generation and low-temperature distribution during the FSW of Al-Cu joints. It shows the brittle characteristics of the weld joints. The impact strength was high at 0.1625 J/mm^2 at an absorbed energy of 6.5 J and an impact velocity of 5.347 m/sec when maximum tool rotational speed was set at1200 rpm and the feed rate of 20 mm/min with hardened H13 steel tool square configurations. This movement is due to high heat generation, high-temperature distribution, and proper metallurgical bonding, which lead to the ductile characteristics of welded Al-Cu joints.

4. Conclusions

With an understanding of the temperature distribution, comparative studies and readings during FSW of AA6101 and C11000 from the various trials, it has been understood that the FSW process parameters such as feed rate, tool rotational speed, type of FSW tool pin profile, and selection of tool material play a vital role in this experiment to carry out the FSW process. The following statements are highlighted:

(1) In trial 3, a maximum temperature of 293°C was observed in the Al-Cu joint area using a hardened H13 steel tool square pin profile where the high tool rotational speed was 1200 rpm and the feed rate was 20 mm/min. It was concluded that, out of the five trials, this one produced the best weld joint. If the HAZ increases, the stress capability of the material decreases.

(2) In trial 4, a minimum temperature of 270°C was observed in the Al-Cu joint area using a hardened H13 steel tool square pin profile where the low tool rotational speed was 1000 rpm and a 10 mm/min feed rate. Due to the lower temperature at the joints, the structural integrity of the Al-Cu plates was preserved. The heat-affected zones of FSW were lower and did not increase when compared with conventional arc welding techniques.

(3) From the study, during conventional welding techniques, the temperature was found to be 845.16°C, which indicates that the higher temperature of heat-affected zones affects the structural integrity of the workpieces. The heat-affected zones in friction stir welding have lower temperatures when compared with conventional flame welding methods.

(4) The highest ultimate tensile strength of the Al-Cu joint was 95.04 MPa, which shows an improvement in Al-Cu joint efficiency. The above value was less than that of the base plate UTS. Hence, the formation of solid butt joints requires high tool rotational speed and feed rate combinations or low tool rotational speed and high feed rates with different tool offsets.

(5) The Charpy impact strength was high at 0.1625 J/mm^2 (162.5 kJ/m^2) at absorbed energy of 6.5 J, impact velocity of 5.347 m/sec for FSW at 1200 rpm and 20 mm/min for the hardened H13 steel tool with square pin profile. The Vickers microhardness of the nugget zone was found to be an average of 104.63 HV1, which is higher than the base metal of Al and Cu and unevenly distributed.

Data Availability

The data used to support the findings of this study are included within the article. Further data or information is available from the corresponding author upon request.

Conflicts of Interest

The authors declare that there are no conflicts of interest regarding the publication of this article.

References

[1] J. Pratap Kumar, A. Raj, K. Arul, and V. Mohanavel, "A literature review on friction stir welding of dissimilar materials," *Materials Today Proceedings*, vol. 47, pp. 286–291, 2021.

[2] M. Shunmugasundaram, A. Praveen Kumar, L. Ponraj Sankar, and S. Sivasankar, "Optimization of process parameters of friction stir welded dissimilar AA6063 and AA5052 aluminum alloys by Taguchi technique," *Materials Today Proceedings*, vol. 27, pp. 871–876, 2020.

[3] A. Raj, J. Pratap Kumar, A. Melwin Rego, and I. SunitRout, "Optimization of friction stir welding parameters during joining of AA3103 and AA7075 aluminium alloys using Taguchi method," *Materials Today Proceedings*, vol. 46, pp. 7733–7739, 2021.

[4] N. Santhosh and K. Ramesha, "Mechanical and thermal characterization of friction stir weld joints of Al–Mg alloy," *Int. J. Res. Aeronaut. Mech. Eng*, vol. 22-23, 2017.

[5] S. V. Safi, H. Amirabadi, M. K. Besharati Givi, and S. M. Safi, "The effect of preheating on mechanical properties of friction stir welded dissimilar joints of pure Copper and AA7075 aluminum alloy sheets," *International Journal of Advanced Manufacturing Technology*, vol. 84, no. 9-12, pp. 2401–2411, 2015.

[6] G. Padmanaban and V. Balasubramanian, "Selection of FSW tool pin profile, shoulder diameter and material for joining AZ31B magnesium alloy – an experimental approach," *Materials & Design*, vol. 30, no. 7, pp. 2647–2656, 2009.

[7] C. M. Chen and R. Kovacevic, "Parametric finite element analysis of stress evolution during friction stir welding," *Proceedings of the Institution of Mechanical Engineers - Part B: Journal of Engineering Manufacture*, vol. 220, no. 8, pp. 1359–1371, 2006.

[8] I. Ajit Kumar and Dr. M. V. Mallikarjuna, "Thermal analysis of friction stir welding," *International Journal of Engineering Research and Technology*, vol. 4, no. 2, pp. 1–5, 2015.

[9] M. Akbari, M. R. M. Aliha, S. M. E. Keshavarz, and A. Bonyadi, "Effect of tool parameters on mechanical properties, temperature, and force generation during FSW," *Proceedings of the Institution of Mechanical Engineers - Part L: Journal of Materials: Design and Applications*, vol. 233, no. 6, pp. 1033–1043, 2016.

[10] A. Ghiasvand, M. Kazemi, M. Mahdipour Jalilian, and H. Ahmadi Rashid, "Effects of tool offset, pin offset, and alloys position on maximum temperature in dissimilar FSW of AA6061 and AA5086," *International Journal of Mechanical and Materials Engineering*, vol. 15, no. 1, pp. 6–14, 2020.

[11] S. B. Aziz, M. W. Dewan, D. J. Huggett, M. A. Wahab, A. M. Okeil, and T. Warren Liao, "Impact of friction stir welding (FSW) process parameters on thermal modeling and heat generation of aluminum alloy joints," *Acta Metallurgica Sinica*, vol. 29, no. 9, pp. 869–883, 2016.

[12] J. A. Jupri, J. Affi, D. Chandra, and M. Asrofi, "Mechanical and microstructure properties on Al-Cu joint processed by friction stir welding: the effect of tilt angle tool," *Material Science Research India*, vol. 16, no. 1, pp. 56–61, 2019.

[13] R. Anbukkarasi and S. V. Kailas, "Influences of shape of the new interfaces and morphology of the intermetallics on mechanical properties of aluminum AA2024–pure copper joints by friction stir welding," *International Journal of Advanced Manufacturing Technology*, vol. 106, no. 11-12, pp. 5071–5083, 2020.

[14] V. D. Yadav and P. S. G. Bhatwadekar, "Friction stir welding of dissimilar materials between AA6101 aluminium and pure Copper," *International Journal of Engineering Sciences and Research Technology*, vol. 3, no. 12, pp. 505–508, 2014.

[15] N. Sharma, A. N. Siddiquee, Z. A. Khan, and M. T. Mohammed, "Material stirring during FSW of Al-Cu: effect of pin profile," *Materials and Manufacturing Processes*, vol. 33, no. 7, pp. 786–794, 2017.

[16] Y. Wei, H. Li, P. Xiao, and J. Zou, "Microstructure and conductivity of the Al-Cu joint processed by friction stir welding," *Advances in Materials Science and Engineering*, vol. 2020, pp. 1–10, Article ID 6845468, 2020.

[17] Sadashiva and Shivanand, "Characteristic investigation on impact strength of aluminium based hybrid composite plates weld by FSW," *International Journal of Engineering & Technology*, vol. 7, no. 3.12, pp. 120–127, 2018.

[18] K. Arul and S. K. Vs, "Magnetorheological based minimum quantity lubrication (MR-MQL) with additive n-CuO,"

Materials and Manufacturing Processes, vol. 35, no. 4, pp. 405–414, 2020.

[19] A. Kulandaivel and S. Kumar, "Effect of magneto rheological minimum quantity lubrication on machinability, wettability and tribological behavior in turning of Monel K500 alloy," *Machining Science and Technology*, vol. 24, no. 5, pp. 810–836, 2020.

[20] T. Kanagaraju, L. G. Babu, V. M. Madhavan et al., "Experimental analysis on drilling of super duplex stainless steel 2507 (SDSS 2507) using cryogenic LCO2 and MQL process," *Biomass Conv. Bioref.*, 2022.